Two-step electrosynthesis and catalytic activity of $CoO—CoO \cdot xH_2O$-supported Ag, Au, and Pd nanoparticles

R. R. Fazleeva,[a] G. R. Nasretdinova,[a] Yu. N. Osin,[b] A. Yu. Ziganshina,[a] and V. V. Yanilkin[a]★

[a]*Arbuzov Institute of Organic and Physical Chemistry, Federal Research Center "Kazan Scientific Center of the Russian Academy of Sciences," 8 ul. Akad. Arbuzova, 420088 Kazan, Russian Federation. Fax: +7 (843) 275 2253. E-mail: yanilkin@iopc.ru*
[b]*Kazan (Volga Region) Federal University, Interdisciplinary Center for Analytical Microscopy, 18 ul. Kremlevskaya, 420018 Kazan, Russian Federation*

Two-step electrosynthesis of $CoO—CoO \cdot xH_2O$-supported metal nanoparticles (MNPs, M = Au, Ag, Pd) was carried out in *N*,*N*-dimethylformamide in the absence and in presence of poly(*N*-vinylpyrrolidone) (PVP) using atmospheric oxygen as both a reagent and a mediator at potentials of its reduction to a superoxide radical anion. In the first step, oxygen reduction in the presence of Co^{2+} ions added to the solution as a salt or generated by dissolving the Co-anode during electrolysis produces a mixture of cobalt oxide CoO and its hydrated form $CoO—CoO \cdot xH_2O$ (CoO_xH_y). When Ag^+, Au^+, Pd^{2+} ions are added to the obtained solution of CoO_xH_y, a redox reaction between CoO and the metal ion gives the MNPs and CoO^+. In the second step, oxygen-mediated electroreduction of CoO^+ serving as the second mediator is carried out, and the redox reaction is completely shifted towards the formation of MNPs. In the absence of PVP, AgNPs (18±4 nm) bind and stabilize completely in the CoO_xH_y matrix, PdNPs (6±1 nm) stabilize only partially, and AuNPs (21±10 nm) do not bind and, therefore, only their agglomerates are obtained (~200 nm). In the presence of PVP, individual AgNPs (5±2 nm), AuNPs (13±5 nm), PdNPs (3±1 nm) are stabilized in the PVP shell and are bound by the matrix. The obtained nanocomposites M/CoO_xH_y and $M@PVP/CoO_xH_y$ catalyze the reduction of *p*-nitrophenol with sodium borohydride in an aqueous medium. Their catalytic activity is due to MNPs; CoO_xH_y acts as an inert matrix.

Key words: electrochemical synthesis, oxygen-mediated electroreduction, cobalt(II) oxide, nanocomposite.

Pseudo-homogeneous metal nanocatalysts, namely metal nanoparticles (MNPs), which are unstabilized or stabilized in solution by binding in the stabilizer shell or on the surface of stable carrier nanoparticles, are of undoubted interest in the development of energy- and resource-saving ecologically safe technologies for obtaining substances and materials for practical use. Unlike classical heterogeneous catalysts, pseudo-homogeneous nanocatalysts have a more developed surface. Due to their high polydispersity, nanosized catalysts are evenly distributed in the medium and, therefore, the catalytic reaction proceeds throughout the entire bulk of the reaction solution. As a result, these catalysts have a higher specific catalytic activity and lack most of the diffusion restrictions characteristic of heterogeneous reactions. A positive aspect of immobilizing MNPs on the surface of larger carrier particles is the ease of separation of the catalyst after the completion of the catalytic reaction by filtration or centrifugation, as well as by application of external magnetic field in the case of magnetically active carriers.

Various NPs can be used as carriers of MNPs, in particular, nano-sized metal oxides.[1—13] Metal oxides catalyze many reactions (oxidation, reduction, coupling with the formation of C—C and C—O bonds, condensation, *etc.*),[5,14—20] therefore, they can serve not only as carriers and stabilizers of MNPs, but also as active co-catalysts, granting the composite bifunctionality or a synergistic effect. These nanocomposites are obtained mainly by chemical reduction of metal ions (complexes) (M^1) with various reducing agents in the presence of other metal oxides[5—7] (M^2) that gives a stoichiometric amount of the oxidized form of the reducing agent as waste. An electrochemical method of producing nanocomposites M^1/M^2O_x is also known, which consists in dispersing the metal of the M^1 electrode during electrolysis under an alternating current in the presence of introduced or electrochemically

Published in Russian in *Izvestiya Akademii Nauk. Seriya Khimicheskaya,* No. 2, pp. 0241—0254, February, 2020.

generated metal oxides (hydroxides) M^2O_x (Al_2O_3, TiO_2, NiO, SnO_2).[8–11] However, this method is carried out at high potentials, is associated with the evolution of hydrogen, and at the present time is limited only to nanocomposites based on PtNPs.

Recently* we proposed a two-step electrosynthesis of nanocomposites M^1/M^2O_x with the use of atmospheric oxygen as a reagent in the first step and as a mediator in the second step at potentials of its reduction to a superoxide radical anion. The high efficiency of this method was demonstrated by the electrosynthesis of silver nanoparticles (AgNPs) on a $CoO—CoO \cdot xH_2O$ matrix in *N*,*N*-dimethylformamide. During the first step, the reduction of oxygen dissolved in air (~2.9 m*M*) in the presence of Co^{2+} ions added to the solution as a salt or generated by dissolving the Co-anode upon electrolysis produced a mixture of cobalt oxide CoO and its hydrated form $CoO \cdot xH_2O$. When Ag^+ ions were added to the obtained $CoO—CoO \cdot xH_2O$ solution, an equilibrium redox reaction between CoO and Ag^+ took place, followed by the formation of AgNPs and CoO^+. During the second step, oxygen-mediated electroreduction of CoO^+ was carried out, and the redox reaction shifted completely toward the formation of AgNPs. The obtained spherical AgNPs were bound and stabilized in the $CoO—CoO \cdot xH_2O$ matrix. Both steps proceeded quantitatively when transmitting a theoretical amount of electricity. This process proceeds at low potentials of reduction of environmentally safe oxygen under mild conditions at room temperature, does not lead to the formation of wastes that are inevitable during chemical synthesis of metal oxides and NPs, is not accompanied by the evolution of hydrogen, and, therefore, appears very promising.

In this regard, in the present work we investigated the possibility of obtaining nanocomposites $Au/CoO—CoO \cdot \cdot xH_2O$ and $Pd/CoO—CoO \cdot xH_2O$ using this method both in the absence and in the presence of poly(*N*-vinylpyrrolidone) (PVP, 40000 Da) as the stabilizer of MNPs. When selecting metals (Au, Pd) and synthesis conditions, the previously described electrosynthesis of AuNPs[21,22] and PdNPs[22,23] by oxygen-mediated reduction of Au^+ and $[PdCl_4]^{2-}$ was taken into account. Since Au^+ and $[PdCl_4]^{2-}$ undergo reduction very easily, we assumed that the redox reaction between CoO and these ions would lead to AuNPs, PdNPs, and CoO^+ by analogy with the reduction of Ag^+. Therefore, nanocomposites obtained by addition of these ions to the $CoO—CoO \cdot xH_2O$ solutions were also included in the present study. Nanocomposites $Ag/CoO—CoO \cdot xH_2O$ were found to exhibit catalytic activity in the reduction of *p*-nitrophenol with sodium borohydride in an aqueous medium, which increased in the presence of micelle-forming cationic surfactant cetyltrimethylammonium chloride (CTAC).* The catalytic activity of the nanocomposites obtained in this work was tested using the same model reaction.

* Hereinafter, the authors refer to the results that will be published in the work V. V. Yanilkin, R. R. Fazleeva, G. R. Nasretdinova, Yu. N. Osin, A. T. Gubaidullin, A. Yu. Ziganshina, Two-step one-pot electrosynthesis and catalytic activity of the xCoO—yCo(OH)$_2$-supported silver nanoparticles, *J. Electrochem. Soc.*, 2020 (in press); http://jes.ecsdl.org/).

Experimental

The studies were carried out by cyclic voltammetry (CV), microelectrolysis, preparative electrolysis, scanning and transmission electron microscopy (SEM and TEM), UV-Vis spectroscopy, and dynamic light scattering (DLS).

Commercially available salts $Co(BF_4)_2 \cdot 6H_2O$, $AgNO_3$, AuCl, $PdCl_2$, Bu_4NBF_4 (Aldrich), PVP (40000 Da) (Alfa Aesar), and CTAC (Acros Organics) were used without additional purification.

Cyclic voltammograms were recorded using a P-30S potentiostat (without IR compensation) (Elins, Russia). The working electrode was a glassy carbon (GC) disk electrode (d = 2 mm) soldered into glass. The electrode was cleaned by mechanical polishing before each measurement. The auxiliary electrode was a Pt-wire. The potentials were measured relative to the saturated calomel electrode (SCE), connected to the test solution by a bridge with a supporting electrolyte and having a potential of −0.41 V relative to E_0' (Fc^+/Fc). The temperature was 295 K.

Preparative electrolysis was carried out in a divided (sintered glass) and an undivided three-electrode glass cells in the potentiostatic mode at room temperature (295 K) using a P-30S potentiostat. The solution was stirred with a magnetic stirrer during electrolysis. The working electrode was a GC-plate (S = 3.2 cm^2), the reference electrode was a SCE connected to the test solution by a bridge with a supporting electrolyte, the auxiliary electrode was a Pt-wire in the case of divided electrolysis, a Co-plate and a Pd-wire in the case of undivided electrolysis. The solvent was DMF, the supporting electrolyte was 0.1 *M* Bu_4NBF_4 and 0.1 *M* Bu_4NCl in the synthesis of PdNPs. Supporting electrolyte solution was placed into the auxiliary anode compartment for divided electrolysis. Metal ions were introduced as salts for divided electrolysis. The obtained particles of cobalt(II) oxide with its hydrated form ($CoO—CoO \cdot xH_2O$) and silver, gold, and palladium nanoparticles were denoted as CoO_xH_y and Ag/CoO_xH_y, Au/CoO_xH_y, and Pd/CoO_xH_y, respectively. During undivided electrolysis, metal ions were generated in the solution during electrolysis by dissolution of the anode metal, and the obtained particles were denoted as $CoO_xH_y^{an}$ and Pd^{an}. Electrosynthesis of CoO_xH_y and $CoO_xH_y^{an}$ was carried out by the known procedure.* The solutions obtained after the addition of Ag^+, Au^+, and $[PdCl_4]^{2-}$ ions to the solutions of CoO_xH_y and $CoO_xH_y^{an}$ (Table 1, runs *1*, *3*, *7*, *9*, and *11*) and after the completion of the subsequent electrolysis (runs *2*, *4*, *8*, *10*, and *12*) were investigated by CV on an indicator GC-electrode (2 mm) directly inside the electrolyzer.

Nanocomposite $Au/CoO_xH_y^{an}$. To a 4 m*M* solution of CoO_xH_y in DMF/0.1 *M* Bu_4NBF_4 (24 mL), AuCl (5.6 mg) was added to achieve a working concentration of 1.5 m*M* and the mixture was sonicated for 40 min to dissolve AuCl (see Table 1, run *1*). Half of the resulting solution (8 mL) was subjected to electroreduction in a divided cell transmitting Q = 1.14 C (1 F based on AuCl) (run *2*).

Table 1. Conditions for the electrosynthesis of nanocomposites

Run	Nanocomposite	C_{CoO}	C_M	Q^a/F	CE^b (%)	References
		mmol L^{-1}				
1	$Au/CoO_xH_y^{an}$	4.0	1.5	2	135	—[c]
2	$Au/CoO_xH_y^{an}$	4.0	1.5	3	100	—[c]
3	$Pd/CoO_xH_y^{an}$	3.3	1.5	2	110	—[c]
4	$Pd/CoO_xH_y^{an}$	3.3	1.5	4	100	—[c]
5	$Pd^{an}/CoO_xH_y^{an}$	4.0	2.3	4	130 (Co^{2+}), 150 (Pd^{2+})	—[c]
6	CoO_xH_y/PVP	3.0	1.5	2	—	—[c]
7	Ag@PVP/CoO_xH_y	3.0	1.5	2	—	—[c]
8	Ag@PVP/CoO_xH_y	3.0	1.5	3	—	—[c]
9	$Au@PVP/CoO_xH_y^{an}$	3.3	1.5	2	110	—[c]
10	$Au@PVP/CoO_xH_y^{an}$	3.3	1.5	3	100	—[c]
11	$Pd@PVP/CoO_xH_y^{an}$	3.7	1.5	2	125	—[c]
12	$Pd@PVP/CoO_xH_y^{an}$	3.7	1.5	4	100	—[c]
13	CoO_xH_y	3.0	—	2	—	*
14	$Ag/CoO_xH_y^{an}$	3.0	1.5	2	100	*
15	$Ag/CoO_xH_y^{an}$	3.0	1.5	3	100	*
16	Pd@PVP	—	1.5	2	100	23
17	Pd@CTAC	—	1.5	2	100	24
18	Ag@CTAC	—	1.5	1	100	24
19	Pd/*p*(MVCA^{8+}-*co*-St)[d]	—	1.5	2	100	25

[a] The amount of transmitted electricity based on 3 m*M* Co^{2+} and/or 1.5 m*M* Ag^+, Au^+, Pd^{2+}.
[b] Metal ion current yield at anodic dissolution of metal.
[c] This work.
[d] *p*(MVCA^{8+}-*co*-St) is a copolymer of tetraviologen calix[4]resorcinol with styrene.

Nanocomposite Pd/$CoO_xH_y^{an}$. To a 3 m*M* solution of CoO_xH_y in DMF/0.1 *M* Bu_4NCl (16 mL), $PdCl_2$ (4.2 mg) was added to achieve a working concentration of 1.5 m*M* and the mixture was sonicated for 40 min to dissolve $PdCl_2$ (see Table 1, run *3*). Half of the obtained solution (8 mL) was subjected to electroreduction in a divided cell transmitting Q = 2.32 C (2 F based on $PdCl_2$) (see Table 1, run *4*).

Nanocomposite $Pd^{an}/CoO_xH_y^{an}$ was obtained by undivided electrolysis of a 3 m*M* solution of $CoO_xH_y^{an}$ in DMF/0.1 *M* Bu_4NCl (10 mL) using a Pd-anode (2.5 cm^2) transmitting Q = 2.94 C (see Table 1, run *5*).

Nanocomposite Ag@PVP/CoO_xH_y. To a solution of 3 m*M* CoO_xH_y and 20 m*M* PVP in DMF/0.1 *M* Bu_4NBF_4 (16 mL) (see Table 1, run *6*), $AgNO_3$ (4.1 mg) was added to achieve a working concentration of 1.5 m*M*) (run *7*). Half of the obtained solution (8 mL) was subjected to electroreduction in a divided cell transmitting Q = 1.14 C (1 F based on Ag^+) (run *8*).

Nanocomposite Au@PVP/$CoO_xH_y^{an}$. To a solution of 3 m*M* $CoO_xH_y^{an}$ and 20 m*M* PVP (35.5 mg) in DMF/0.1 *M* Bu_4NBF_4 (16 mL), AuCl (5.6 mg) was added to achieve a working concentration of 1.5 m*M* and the mixture was sonicated for 40 min (see Table 1, run *9*). Half of the obtained solution (8 mL) was subjected to electroreduction in a divided cell transmitting Q = 1.14 C (1 F based on AuCl) (run *10*).

Nanocomposite Pd@PVP/$CoO_xH_y^{an}$. To a solution of 3 m*M* $CoO_xH_y^{an}$ and 20 m*M* PVP (35.5 mg) in DMF/0.1 *M* Bu_4NCl (16 mL), $PdCl_2$ (4.2 mg) to achieve a working concentration of 1.5 m*M* was added and the mixture was sonicated for 40 min (see Table 1, run *10*). Half of the obtained solution (8 mL) was subjected to electroreduction in a divided cell transmitting Q = 2.32 C (2 F based on $PdCl_2$) (run *11*).

After the completion of electrolysis, the obtained solutions were studied by CV, UV-Vis spectroscopy, DLS; additionally, the catalytic activity of the obtained dispersions of nanocomposites was tested.

To study the particles formed during electrolysis by SEM, TEM, DLS, and UV-Vis spectroscopy, they were either precipitated by centrifugation (15000 rpm, 2 h), washed once with DMF and twice with ethanol (see Table 1, runs *1—5*), or the solvent was removed *in vacuo* and the precipitate was washed trice with ethanol to remove the supporting electrolyte and other soluble components (runs *6—12*). Washing was carried out as follows: the nanoparticles were dispersed in a solvent by sonication and then precipitated by centrifugation (15000 rpm, 1 h (runs *1—5*) or 3 h (runs *6—12*)). The resulting precipitate was dispersed in ethanol by sonication.

Electron microscopy. For investigation by SEM, the obtained colloidal solution of NPs was applied onto the surface of a titanium foil preliminarily cleaned by sonication in water, acetone, and ethanol, and the sample was dried at room temperature. A Merlin field emission scanning electron microscope (Carl Zeiss, Germany) was used. Surface morphology was studied in the secondary electron (SE) mode with an accelerating voltage of primary electrons equal to 5 kV and a probe current equal to 300 pA to minimize impact on the sample. The accelerating voltage of primary electrons was 20 kV and the probe current was 1 nA for the detection of phase contrast and microprobe elemental analysis. The angle selective backscattered (AsB) detector was used. The microscope was equipped with an AZtec X-MAX energy-dispersive spectrometer (Oxford Instruments, UK). Spectrometer resolution was 127 eV. Measurement accuracy was 0.01—1.00%. Elemental analysis was carried out at an accelerat-

ing voltage of 20 keV and a working length of 9.6 mm, which made it possible to minimize errors. Probe depth was less than 1 μm. Quantitative analysis was performed using a reference standard for X-RAY microanalysis implemented in AZteC software (Registered Standard No. 8842).

For investigation by TEM, 5 μL of the solution was applied to a formvar/carbon coated copper grid with a diameter of 3 mm (Formvar/Carbon, Lacey Formvar) and dried at room temperature. After drying, the grid was placed in a transmission electron microscope using a special graphite holder for microanalysis. Transmission electron microscopy was carried out in the HR-TEM mode using a Hitachi HT 7700 Excellence transmission electron microscope (Japan) at an accelerating voltage of 100 keV with a resolution of 0.144 nm. Elemental analysis was carried out using an Oxford Instruments X-Max^n 80T console (UK) with a special holder.

UV-Vis electronic absorption spectra were recorded on a Perkin-Elmer Lambda 25 spectrometer (USA).

Catalytic reduction of *p*-nitrophenol with sodium borohydride in the presence of synthesized nanocomposites. An aqueous solution (1.5 mL) containing 0.1 mmol L^{-1} of *p*-nitrophenol and 5 m*M* $NaBH_4$ was placed into a quartz cell (l = 0.5 cm), and a dispersion of nanocomposites (2 μL) obtained by electrolysis in DMF was added. The reaction was carried out at 295 K, the reaction progress was monitored using the change in the optical density of *p*-nitrophenol at 400 nm over time.

Results and Discussion

Electrosynthesis of all nanocomposites was carried out in two steps using dissolved atmospheric oxygen as a reagent in the first step and as a mediator in the second step with controlled potentials of its reduction to the superoxide radical anion $O_2^{\bullet -}$ (E = –0.95 V rel. SCE). No products were deposited on the cathode during electrolysis, as indicated by the unchanged weight of the electrode before and after electrolysis. In the first step, solutions of CoO_xH_y or $CoO_xH_y^{an}$ with a concentration of 3.0—4.0 mmol L^{-1} were obtained as described* (see Table 1). The course of electrolysis, the color, the consistency, the UV-Vis absorption spectra, the results of DLS and CV studies of the obtained CoO_xH_y and $CoO_xH_y^{an}$ solutions entirely corresponded to the previously described results for these particles, therefore, no additional studies were carried out to verify their composition and structure. Then Au^+, Pd^{2+}, Ag^+ ions were added to the CoO_xH_y and $CoO_xH_y^{an}$ solutions as salts and the second reduction step was carried out. During the second step, Pd^{2+} ions were also obtained in the solution by anodic dissolution of the Pd-electrode.

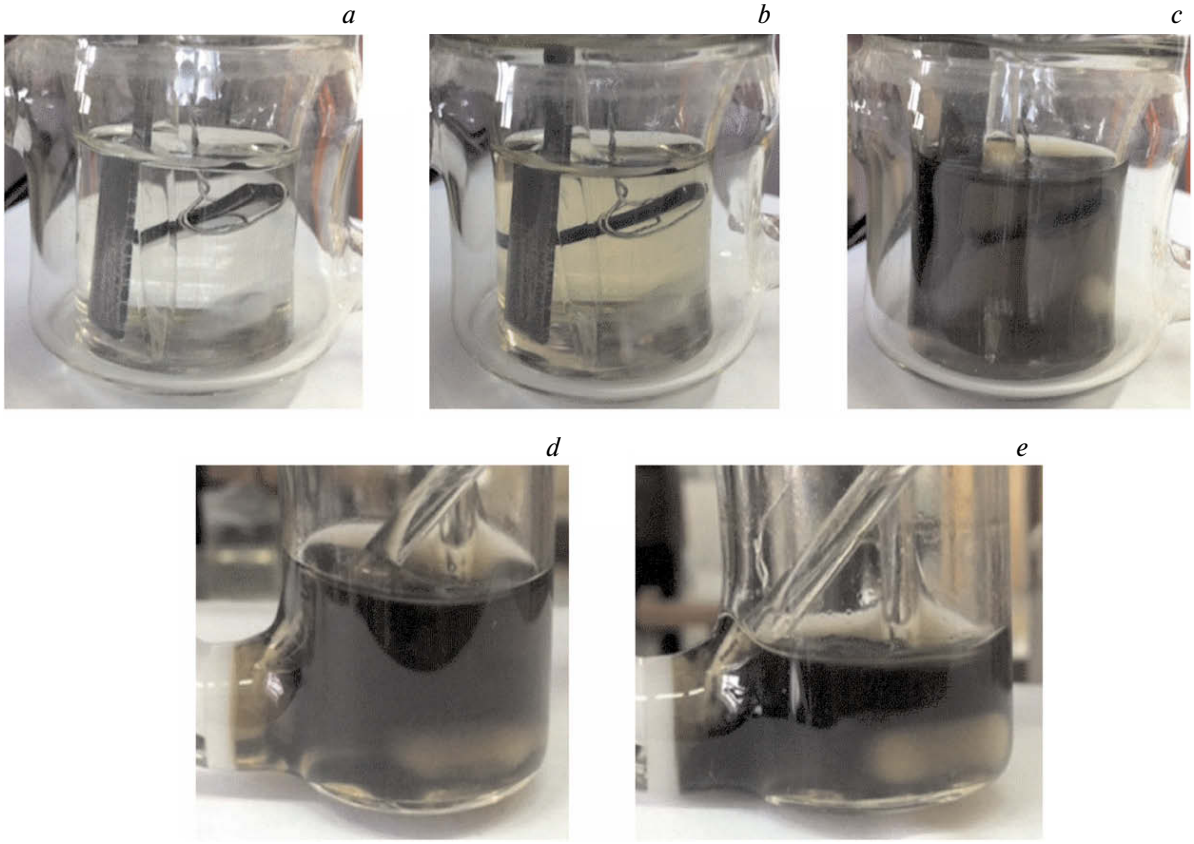

Fig. 1. Images of the electrolysis cell taken during electrolysis of the system ~2.9 m*M* O_2/Co-anode at E = –0.95 V in a DMF/0.1 *M* Bu_4NBF_4 medium for different amounts of transmitted electricity (based on Co^{2+}): 0 (*a*), 0.2 (*b*), and 2.0 F (*c*), after addition 1.5 m*M* AuCl to the obtained solution and sonication for 40 min (run *1*) (*d*), and after the subsequent reduction at E = –0.95 V (1 F based on AuCl) (run *2*) (*e*).

Note. Figures 1 and 8 are available in full color on the web page of the journal (http://link.springer.com/journal/11172).

Electrosynthesis of M/$CoO_xH_y^{an}$ (M = Au, Pd). Addition of AuCl (1.5 m*M*) to a 4 m*M* solution of $CoO_xH_y^{an}$ led to no visual changes. Gold chloride is poorly soluble in DMF, and the mixture was sonicated for 40 min to increase its solubility (see Table 1, run *1*). However, no noticeable changes occurred even after sonication (Fig. 1, *d*). There is no AuCl reduction peak on the CV curve, which is usually appeared in the potential range −0.1—0.0 V depending on the state of the electrode surface,[21,26] and only oxygen reduction and CoO (A^{CoO}) (E = 0.58 V) oxidation peaks are observed (Fig. 2). The intensity of these peaks does not change over time, but the current of the first oxygen reduction peak ($C_1^{O_2}$) is 25% higher than in the absence of AuCl. After the subsequent reduction at a controlled potential of E = −0.95 V transmitting Q = 1 F based on AuCl (run *2*), the color of the solution and the morphology of the CV curve remained the same, but the current of the first oxygen reduction peak decreased to the initial value, *i.e.*, to its value in the absence of AuCl (see Fig. 2).

The solutions obtained in runs *1* and *2* (see Table 1), as well as the particles formed during these experiments and precipitated by centrifugation and dispersed in ethanol were studied by several physicochemical methods. The sizes of the Au/$CoO_xH_y^{an}$ particles in the solution determined by DLS (Fig. 3, *a*) and their UV-Vis absorption spectra (Fig. 3, *b*) correspond to the $CoO_xH_y^{an}$ particles, and the characteristic absorption band, which is caused by the surface plasmon resonance of AuNPs and is usually observed in the region of 500—600 nm,[27] was not detected. According to SEM and TEM, as well as energy dispersive X-ray spectroscopy (Fig. 4), only large agglomerates (with sizes larger than 200 nm) of gold nanoparticles were obtained in runs *1* and *2* (Table 2) with average sizes of 20±5 nm (run *1*) and 21±10 nm (run *2*), deposited together with $CoO_xH_y^{an}$, while isolated AuNPs were not formed.

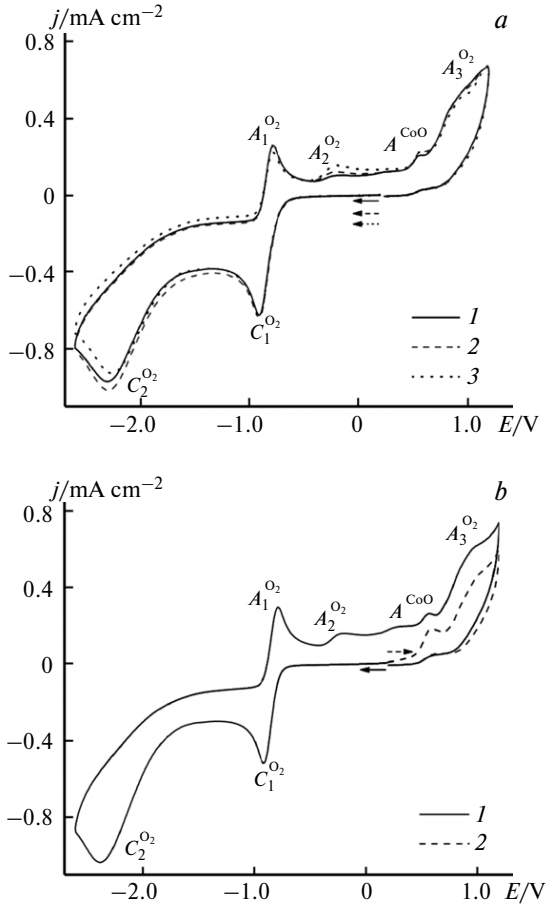

Fig. 2. CV curves of the system O_2 (~2.9 m*M*)/$CoO_xH_y^{an}$ (4 m*M*)/AuCl (1.5 m*M*) in a DMF/0.1 M Bu_4NBF_4. *a*, After 5 (*1*), 60 (*2*), and 180 min (*3*) of sonication and *b*, after subsequent reduction at E = −0.95 V (Q = 1 F based on Au^+) with an initial potential cathodic (*1*) and anodic (*2*) sweeps. The potential sweep rate is ν = 100 mV s^{-1}. *C* are the reduction peaks, *A* are the oxidation peaks. Potentials *E* are given relative to the potential of SCE.

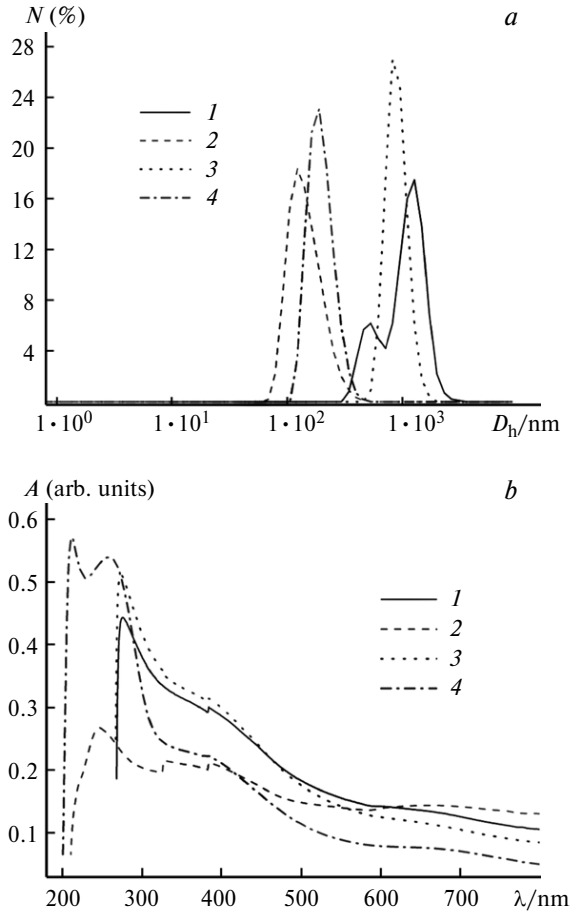

Fig. 3. Size distribution diagram (DLS results) (*a*) and UV-Vis absorption spectra (*b*) of Au/$CoO_xH_y^{an}$ particles obtained in run *1* (*1, 2*) and *2* (*3, 4*): *1*, *3*, in solutions after electrolysis and *2*, *4*, isolated and dispersed in ethanol (see Table 1 and Experimental section). N is the number of particles, D_h is the average hydrodynamic diameter of the particles.

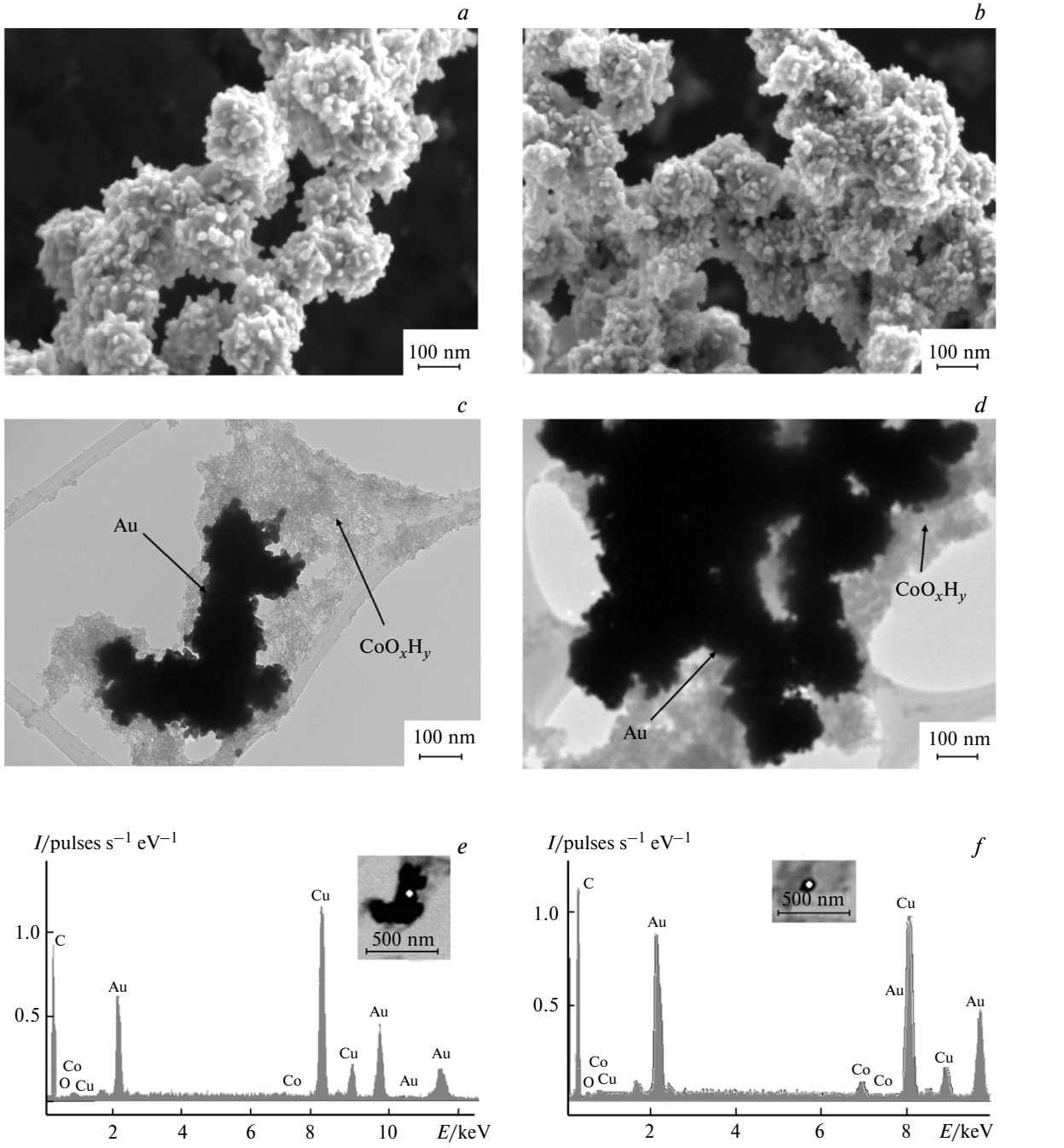

Fig. 4. SEM (*a*, *b*) and TEM images (*c*, *d*), as well as energy dispersive spectra (*e*, *f*) of Au/$CoO_xH_y^{an}$ particles obtained in runs *1* and *2*. The Cu lines correspond to the support. The insets in figures *e* and *f* show the areas of analysis.

From the obtained results, it follows that (1) AuNPs already partially or quantitatively form after the addiution of Au^+ ions to the solution of $CoO_xH_y^{an}$ as a result of a redox reaction between CoO and Au^+ (Scheme 1); (2) the increase in current of the first oxygen reduction peak in run *1* is due to oxygen-mediated reduction of the residual amounts of Au^+ and/or CoO^+ bound in the matrix; (3) oxygen-mediated reduction of CoO^+ and the complete reduction of Au^+ takes place during the second reduction step (see Scheme 1); (4) the $CoO_xH_y^{an}$ matrix does not stabilize AuNPs, but it binds and stabilizes individual silver nanoparticles;* 5) the absence of a plasmon resonance of AuNPs is due to the lack of these particles in the solution.

Electrosynthesis and study of the nanocomposite Pd/$CoO_xH_y^{an}$ was carried out as described for the nanocomposite Au/$CoO_xH_y^{an}$. Solid $PdCl_2$ was added to the 3.3 m*M* solution of $CoO_xH_y^{an}$ in DMF/0.1 *M* Bu_4NCl obtained in the first step and the mixture was sonicated

Table 2. Properties of nanocomposites

Run	Nanocomposite	Size[a]/nm			λ_{max}[b]/nm	Catalytic activity[c]		Reference
		DLS	SEM[d]	TEM[d]		k_1/s^{-1}	k_2/L mol^{-1} s^{-1}	
1	$Au/CoO_xH_y^{an}$	525[d], 1283[d], 123[e]	—	20±5	—	$4.9\cdot10^{-4}$	$2.5\cdot10^{2}$	—[f]
2	$Au/CoO_xH_y^{an}$	853[d], 191[e]	—	21±10	—	$1.9\cdot10^{-4}$	$9.5\cdot10^{1}$	—[f]
3	$Pd/CoO_xH_y^{an}$	105[d], 105[e]	—	4±1	—	$4.2\cdot10^{-3}$	$2.1\cdot10^{3}$	—[f]
4	$Pd/CoO_xH_y^{an}$	120[d], 50[d], 106[e]	—	6±1	—	$8.5\cdot10^{-3}$	$4.3\cdot10^{3}$	—[f]
5	$Pd^{an}/CoO_xH_y^{an}$	30[d], 89[d], 31[d], 90[e]	—	8±3	—	$9.7\cdot10^{-3}$	$4.9\cdot10^{3}$	—[f]
6	CoO_xH_y/PVP	8—21[d], 91[e]	—	—	—	$9.1\cdot10^{-6}$	—	—[f]
7	Ag@PVP/CoO_xH_y	24[d], 71[e]	9±3	6±2	425, 431[d]	$1.4\cdot10^{-3}$	$7.0\cdot10^{2}$	—[f]
8	Ag@PVP/CoO_xH_y	21[d], 91[e]	8±3	5±2	426, 442[d]	$2.0\cdot10^{-4}$	$1.0\cdot10^{2}$	—[f]
9	$Au@PVP/CoO_xH_y^{an}$	—	—	44±16	655	$2.2\cdot10^{-3}$	$1.1\cdot10^{3}$	—[f]
10	$Au@PVP/CoO_xH_y^{an}$	—	—	13±5	565	$1.3\cdot10^{-3}$	$6.5\cdot10^{2}$	—[f]
11	$Pd@PVP/CoO_xH_y^{an}$	—	—	—	—	$9.4\cdot10^{-3}$	$4.7\cdot10^{3}$	—[f]
12	$Pd@PVP/CoO_xH_y^{an}$	—	—	3±1	—	$9.5\cdot10^{-3}$	$4.8\cdot10^{3}$	—[f]
13	CoO_xH_y	50—1283[d], 94[e]	—	—	—	$3.1\cdot10^{-6}$	—	*
14	$Ag/CoO_xH_y^{an}$	50[d], 500[d], 58[e]	—	22±11	437, 420[d]	$9.0\cdot10^{-4}$	$4.5\cdot10^{2}$	*
15	$Ag/CoO_xH_y^{an}$	1281—5560[d], 79[e]	—	18±4	430	$1.2\cdot10^{-3}$	$6.0\cdot10^{2}$	*
16	Pd@PVP	8[d]	44±10	<1—2	—	$3.3\cdot10^{-3}$	$1.7\cdot10^{3}$	23
17	Pd@CTAC	51[d]	14±3	5±1	—	$6.0\cdot10^{-3}$	$3.0\cdot10^{3}$	24
18	Ag@CTAC	8[d], 17[d]	34±11	18±5	405	$2.5\cdot10^{-3}$	$1.2\cdot10^{3}$	24
19	Pd/*p*(MVCA^{8+}-*co*-St)	30—500[d]	85	3—8	—	$1.4\cdot10^{-3}$	$7.0\cdot10^{2}$	25

[a] The average hydrodynamic particle diameter was determined by DLS, the size of MNPs was determined by TEM, and the size of MNPs with the PVP shell was determined by SEM.
[b] Absorption maxima of MNPs in UV-Vis spectra.
[c] Catalytic activity of MNPs in the reduction of *p*-nitrophenol. Reaction conditions: C(*p*-nitrophenol) = 0.1 mmol L^{-1}, $C(NaBH_4)$ = 5 mmol L^{-1}, C(MNPs) = $2\cdot10^{-6}$ mol L^{-1}, $C(CoO_xH_y)$ = 4.0—5.3·10^{-6} mol L^{-1}, C(PVP) = $2.6\cdot10^{-4}$ mol L^{-1}, water (see Experimental section).
[d] Results for NPs isolated and dispersed in ethanol.
[e] Results for NPs in solution after electrolysis.
[f] This work.

Scheme 1

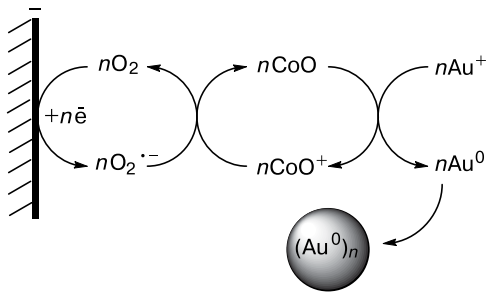

for 40 min to achieve dissolution (see Table 1, run *3*), then electroreduction was carried out at $E = -0.95$ V transmitting Q = 2 F based on $PdCl_2$ (run *4*). The color of the solutions, the sizes of the particles in the solution according to DLS (see Table 2), and the UV-Vis absorption spectrum entirely corresponded to those observed for the synthesis of $Au/CoO_xH_y^{an}$. However, CV curves and SEM and TEM images have their own distinctive features. Thus, the CV curves of the solution obtained in run *3* (Fig. 5) lack the CoO oxidation peak, but there is a reduction peak at

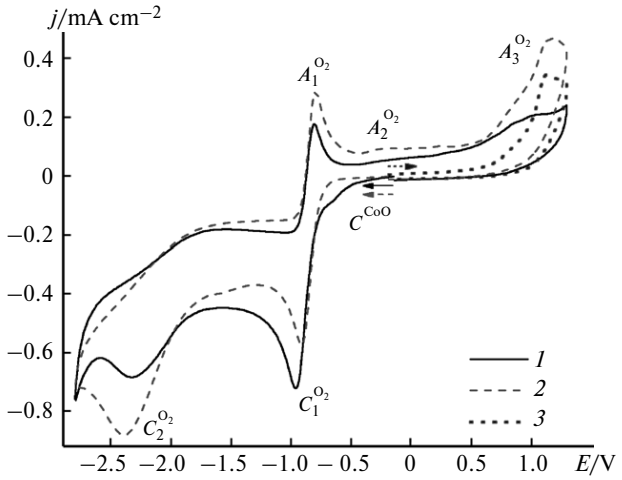

Fig. 5. CV curves of the system O_2 (~2.9 m*M*)/$CoO_xH_y^{an}$ (3 m*M*)/$PdCl_2$ (1.5 m*M*) in a DMF/0.1 M Bu_4NCl before (*1*) and after (*2*, *3*) electrolysis at $E = -0.95$ V (Q = 2.32 C (2 F)) with an initial potential cathodic (*1, 2*) and anodic (*3*) sweeps. The potential sweep rate is ν = 100 mV s^{-1}. *C* are the reduction peaks, *A* are the oxidation peaks. Potentials *E* are given relative to the potential of SCE.

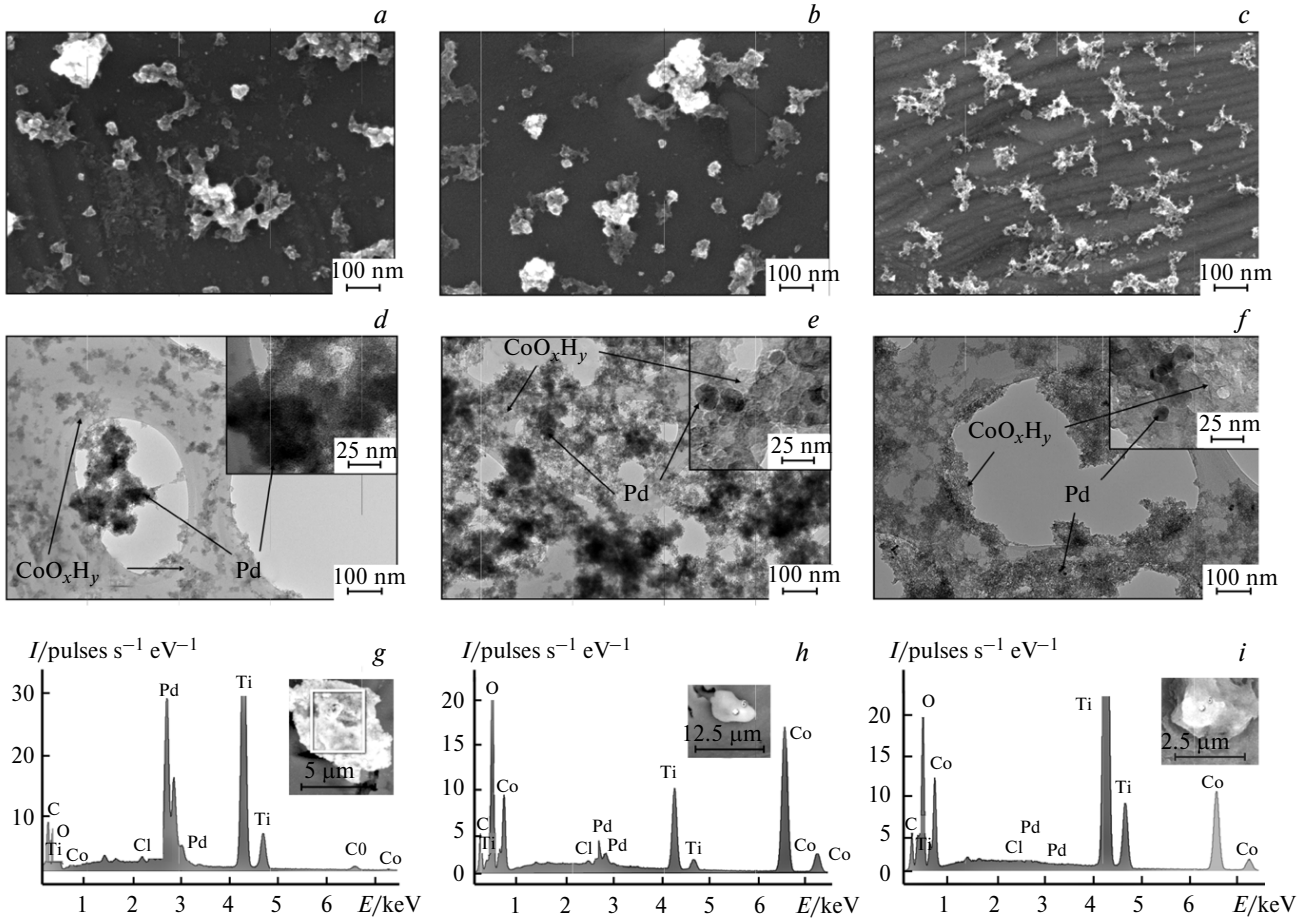

Fig. 6. SEM (*a*—*c*) and TEM images (*d*—*f*), as well as energy dispersive spectra (*g*—*i*) of Pd/$CoO_xH_y^{an}$ and Pd^{an}/$CoO_xH_y^{an}$ particles obtained in runs *3* (*a*, *d*, *g*), *4* (*b*, *e*, *h*), and *5* (*c*, *f*, *i*). The Ti lines correspond to the support. The insets in figures *g*—*i* show the areas of analysis.

E_p = −0.65 V, previously* assigned to CoO^+ reduction. In the presence of a large excess of the chloride ions, $PdCl_2$ exists in the solution mainly as a complex ion $[PdCl_4]^{2-}$.[21] Its reduction and Pd^0 reoxidation peaks observed at −1.48 and 0.57 V, respectively, are absent in the CV curves. The current of the first oxygen reduction peak of is 35% higher than the value recorded in the absence of $PdCl_2$. The current decreases to the value observed in the absence of $PdCl_2$ after the subsequent reduction (run *4*), and the CoO^+ reduction peak also disappears.

Electron microscopy and energy dispersive X-ray microanalysis (Fig. 6) indicate that both individual spherical PdNPs with an average size of 5±2 nm and their larger aggregates bound in a $CoO_xH_y^{an}$ matrix are formed in runs *3* and *4*.

Thus, the syntheses of nanocomposites Pd/$CoO_xH_y^{an}$ and Au/$CoO_xH_y^{an}$ are similar with the only exception that in the first case some of the individual PdNPs bind and stabilize on the $CoO_xH_y^{an}$ matrix.

Electrosynthesis of the nanocomposite Pd^{an}/$CoO_xH_y^{an}$ was carried out in one undivided cell (one-pot synthesis). In the first step, a 3.8 m*M* $CoO_xH_y^{an}$ solution in a DMF/0.1 *M* Bu_4NCl medium was obtained. Then, the Co-anode was replaced with a Pd-anode and the second step of electrolysis was carried out transmitting the theoretically necessary amount electricity to generate and reduce 1.5 m*M* $[PdCl_4]^{2-}$ (see Table 1, run *5*). Effective dissolution of the Pd-anode in this medium upon transmitting this amount of electricity to give the complex dianion $[PdCl_4]^{2-}$ was demonstrated preliminary by electrolysis at a controlled potential of E = 0.60 V. The weight of the Pd-anode decreased during electrolysis in the model experiment, and the CV curves of the obtained solution exhibited the $[PdCl_4]^{2-}$ reduction ($C^{[PdCl_4]^{2-}}$) and the Pd^0 reoxidation peaks ($A^{Pd(0)}$) (Fig. 7).

The CV curve of the solution obtained in run *5* has only the oxygen reduction and reoxidation peaks with the initial intensity and the CoO oxidation peak at the potential E_p = 0.54 V. It is interesting that during electrolysis the weight of the Pd-anode decreased by 50% more than expected from Faraday's law. Apparently, alongside dissolution, the Pd-anode also undergoes dispersion due

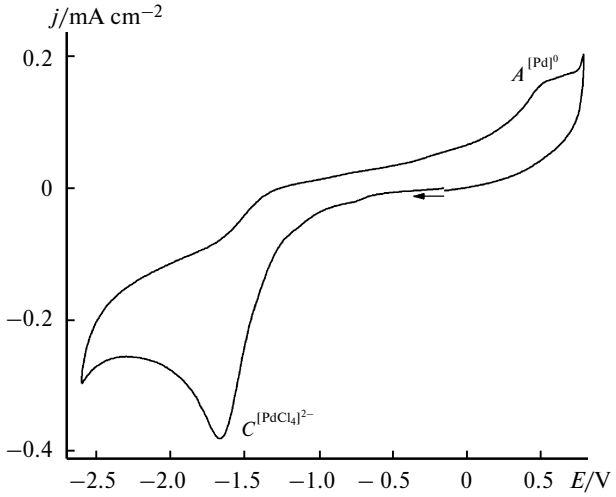

Fig. 7. CV curves in a DMF/0.1 *M* Bu_4NCl after electrolysis with the dissolution of the Pd-anode at $E = 0.60$ V ($Q = 2$ F based on 1.5 m*M* $[PdCl_4]^{2-}$). The potential sweep rate is $\nu = 100$ mV s^{-1}. *C* is the reduction peak, *A* is the oxidation peak. Potentials *E* are given relative to the potential of SCE.

to its nonuniform dissolution, as is in the case of the Ag-anode.[28—31]

A comparison of the characteristics of $Pd^{an}/CoO_xH_y^{an}$ and $Pd/CoO_xH_y^{an}$ composites (see Table 2) and the analysis of the SEM and TEM images, as well as energy-dispersive spectra (see Fig. 6), show that these composites are nearly identical. Only the larger size of individual PdNPs of the $Pd^{an}/CoO_xH_y^{an}$ composite, equal to 8±3 nm, is noteworthy. This is probably due to the dispersion of the Pd-anode, during which the PdNPs larger than those formed during the reduction of $[PdCl_4]^{2-}$ are transferred into the solution.

The obtained results indicate that the $CoO_xH_y^{an}$ matrix does not bind or stabilize PdNPs and AuNPs. Thus, in order to stabilize these NPs, it is necessary to added stabilizers of MNPs to the solution. For this purpose, we selected PVP and CTAC, which are widely used for this purpose. For completeness, AgNPs were also included in the study.

Electrosynthesis of nanocomposites M@PVP/CoO_xH_y (M = Ag, Au, Pd). Electrosynthesis and studies of nanocomposites M@PVP/CoO_xH_y were carried out similarly to the electrosynthesis of M/CoO_xH_y in the absence of PVP. In the first step, reduction of the system O_2 (~2.9 m*M*)/$Co(BF_4)_2$ (3 m*M*)/PVP (20 m*M*) in a divided cell at a controlled potential of the redox pair $O_2/O_2^{\bullet -}$ equal to $E = -0.95$ V yielded a PVP/CoO_xH_y composite (see Table 1, run *6*). During electrolysis, the amount of electricity transmitted was equal to the theoretical amount required for binding radical anions $O_2^{\bullet -}$ with 3 m*M* Co^{2+} ions, to form cobalt(II) oxide in the solution. Electrolysis proceeds similarly as in the absence of PVP,* and, as a result, a slightly cloudy brown solution of CoO_xH_y was obtained (Fig. 8). The UV-Vis spectrum of the solution (Fig. 9) corresponds to CoO_xH_y. According to DLS, the CoO_xH_y particles obtained in the presence of PVP in the starting DMF solution are considerably smaller than that obtained in the absence of PVP. It is obvious that PVP binds and stabilizes nano-sized CoO_xH_y particles. The nanocomposite PVP/CoO_xH_y deposited on the support does not have a specific size and shape, but represents

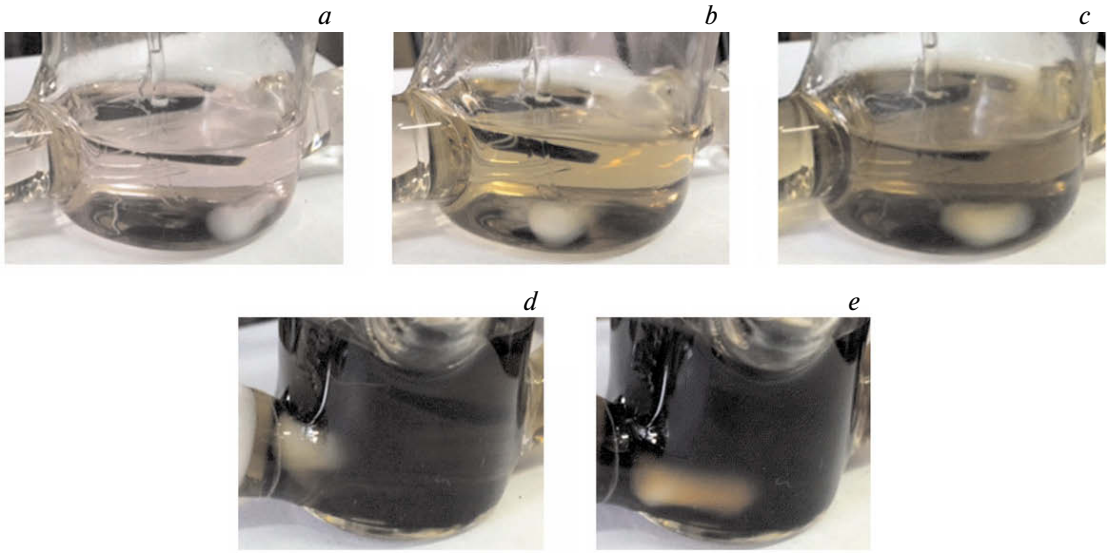

Fig. 8. Images of the electrolysis cell taken during electrolysis of the system O_2 (~2.9 m*M*)/Co^{2+} (3 m*M*)/PVP (20 m*M*) at $E = -0.95$ V in a DMF/0.1 *M* Bu_4NBF_4 medium for different amounts of transmitted electricity (based on Co^{2+}) (run *6*): 0 (*a*), 0.2 (*b*), and 2.0 F (*c*), after addition of 1.5 m*M* $AgNO_3$ to the obtained solution (run *7*) (*d*), and after the subsequent reduction (run *8*) (*e*) (see Table 1 and Experimental section).

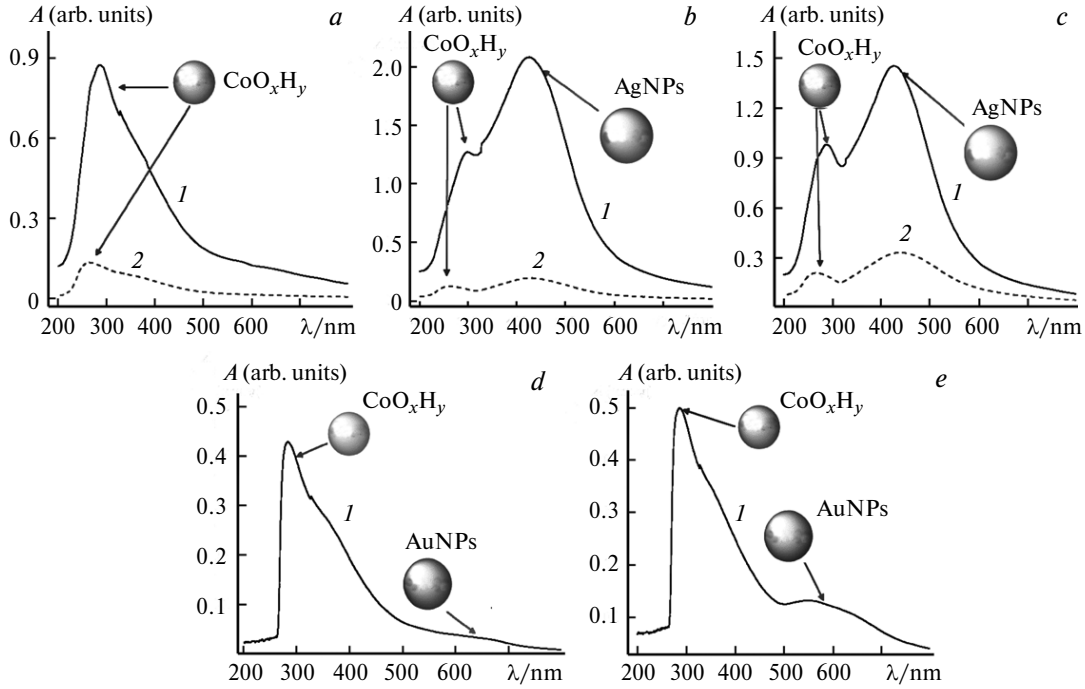

Fig. 9. UV-Vis spectra of nanocomposites obtained in runs *6* (*a*), *7* (*b*), *8* (*c*), *9* (*d*), and *10* (*e*): *1*, in a DMF solution after electrolysis and *2*, isolated NPs dispersed in ethanol.

a general matrix consisting of small CoO_xH_y@PVP particles bound together (Fig. 10).

When an aliquot of a 1.5 m*M* $AgNO_3$ solution is added to the obtained solution of PVP/CoO_xH_y nanocomposite, an equilibrium redox reaction between CoO and Ag^+ occurs to give AgNPs (see Table 1, run *7*, Fig. 8, *d*). Moreover, according to CV, a small portion (4%) of Ag^+ ions is retained even 1 h after the experiment onset, and the current of the first oxygen reduction peak is 33% higher. Upon subsequent reduction at $E = -0.95$ V (run *8*), the oxygen reduction current decreases to the value observed in the absence of Ag^+, and Ag^+ ions are reduced quantitatively. The formation of AgNPs in runs *7* and *8* is evidenced by the surface plasmon resonance of AgNPs[32,33] in the 425—442 nm range (see Fig. 9 and Table 2). The obtained AgNPs have a spherical shape, are encapsulated in the PVP shell, and are bound in the CoO_xH_y matrix in this form (see Fig. 10). The sizes of the AgNPs obtained in runs *7* (6±2 nm) and *8* (5±2 nm) are approximately equal and noticeably smaller than the sizes of AgNPs obtained in the absence of PVP (18±4 nm).*

During a two-step electrosynthesis of nanocomposites Au@PVP/$CoO_xH_y^{an}$ and Pd@ PVP/$CoO_xH_y^{an}$ in the presence of PVP, both the $CoO_xH_y^{an}$ nanoparticles and individual MNPs were bound and stabilized. In contrast to the experiments in the absence of PVP, the PVP/$CoO_xH_y^{an}$ solutions darkened after the addition of AuCl and $PdCl_2$ and sonication, which evidenced in favor of the formation of NPs of these metals by reduction of the Au^+ and $[PdCl_4]^{2-}$ ions with cobalt oxide(II). The direct proof of the formation of AuNPs during this (see Table 1, run *9*) and subsequent (run *10*) reduction steps is a wide absorption band at 560—652 nm caused by a surface plasmon resonance of AuNPs (see Fig. 9).

According to SEM and TEM, as well as energy-dispersive spectroscopy (see Fig. 11), in the presence of PVP the individual AuNPs and PdNPs were obtained. Palladium NPs are spheres with an average size of 3±1 nm (see Table 2, run *12*). Gold NPs obtained in runs *9* and *10* have different shapes (spherical, triangular, and multifaceted) and are polydisperse with sizes 44±16 nm (run *9*) and 13±5 nm (run *10*).

Another widely used stabilizer of MNPs is CTAC, however, it turned out to be completely impossible to obtain M@CTAC/CoO_xH_y nanocomposites. In fact, the CoO_xH_y particles did not form during the electroreduction of the system O_2 (~2.9 m*M*)/$Co(BF_4)_2$ (3 m*M*)/CTAC (20 m*M*) at a controlled oxygen reduction potential to a superoxide radical anion $E = -1.05$ V. When $Co(BF_4)_2$ was added to the solution of supporting electrolyte and CTAC, the solution turned blue; this color is corresponded to the $[CoCl_4]^{2-}$ complex. Electrolysis was accompanied by electrode passivation, and the color of the solution remained almost unchanged during electrolysis ($Q = 2$ F based on $[CoCl_4]^{2-}$). Apparently, CTAC stabilizes the $[CoCl_4]^{2-}$ anions and prevents their reaction with superoxide radical anions to give CoO_xH_y.

Catalytic activity of nanocomposites. The catalytic activity of the obtained nanocomposites was tested in the

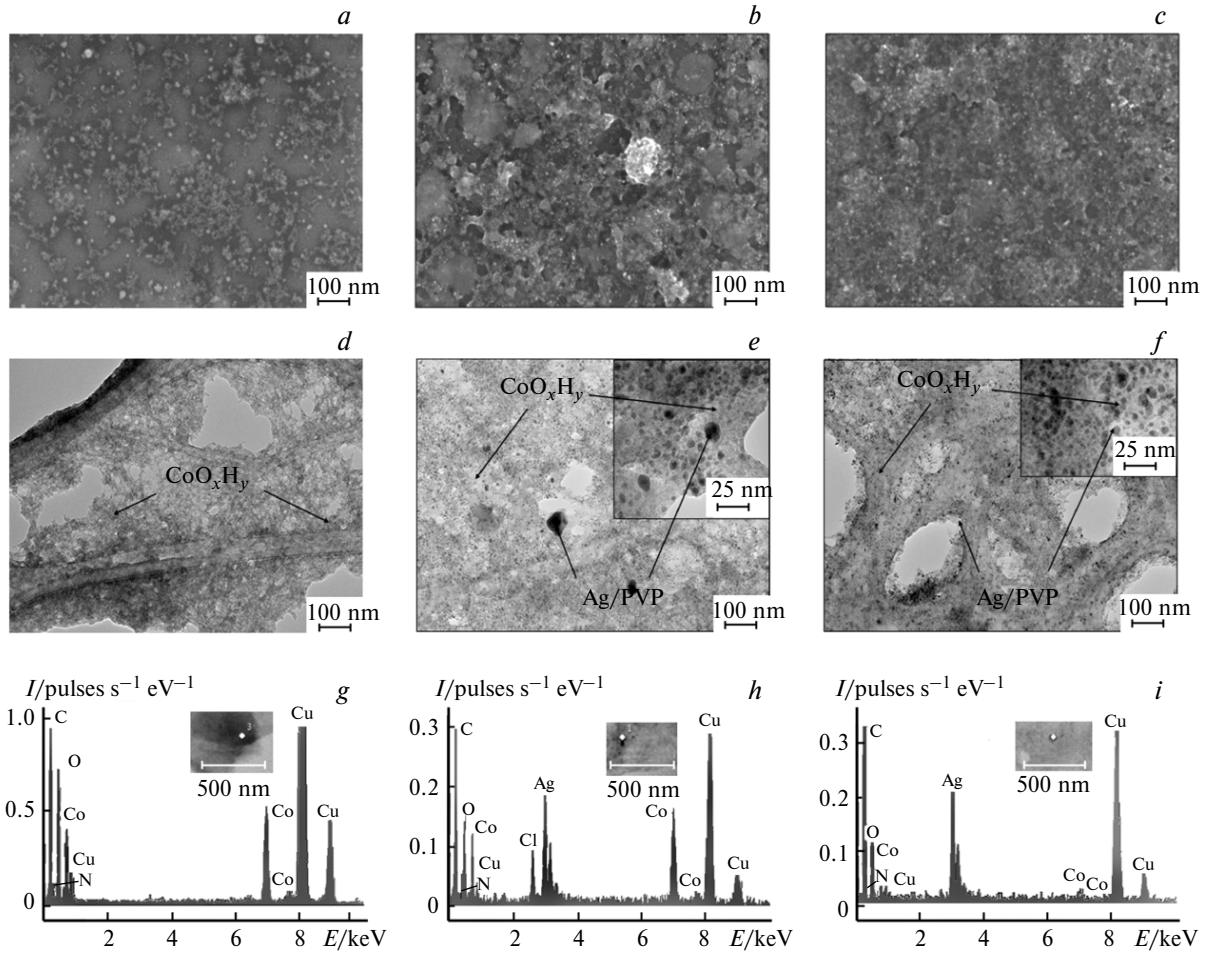

Fig. 10. SEM (*a*—*c*) and TEM images (*d*—*f*), as well as energy-dispersive spectra (*g*—*i*) of the CoO_xH_y/PVP and Ag@CoO_xH_y/PVP nanocomposites obtained in runs *6* (*a*, *d*, *g*), *7* (*b*, *e*, *h*), and *8* (*c*, *f*, *i*) (see Table 1 and Experimental section). The insets in figures *g*—*i* show the areas of analysis. The Ti and Cu lines correspond to the support.

reduction of *p*-nitrophenol with sodium borohydride (Scheme 2), which is catalyzed by both metal nanoparticles[23—25,34—37] and metal oxides TiO_2, Cu_2O, Fe_2O_3.[38,39] An aliquot of the solutions of the nanocomposites obtained during electrolysis was used in the catalytic reaction. The reaction was carried out in water in the presence of a 50-fold excess of sodium borohydride ($NaBH_4$, 5 m*M*). The starting concentration of *p*-nitrophenol was equal to 0.1 mmol L^{-1}. The reaction was monitored by UV-Vis spectroscopy. No reduction of *p*-nitrophenol occurred in the absence of a catalyst.[25,37] When adding the obtained nanocomposites (2 mol.% M based on *p*-nitrophenol), the intensity of the absorption band of the *p*-nitrophenolate ion at the 400 nm range decreases, while the intensity of the absorption band of *p*-aminophenol, the reduction product, at 300 nm increases (Fig. 12). When nanocomposites Pd@PVP/$CoO_xH_y^{an}$ were used as catalysts (see Table 2, runs *10* and *11*), no induction period was observed and the reaction began immediately after addition of the catalyst to the reaction mixture. An induction period was observed when any other catalysts was used. During the induction period, the reaction rate is low, and, according to the works,[40,41] the reagents diffuse toward the surface of the metal or the surface of the catalyst is restructured to adsorb the reagents. The longest induction period was observed for nanocomposites Au/$CoO_xH_y^{an}$ (runs *1* and *2*), which was equal to 24 and 30 min, respectively, while the induction period in the other cases ranged from 7 to 13 min. The reaction rate increases sharply after the induction period. Since a large excess of $NaBH_4$ is used, the catalytic reaction is characterized by a pseudo-first order. The pseudo-first order rate constants (k_1) and the catalytic activity of nanocomposites (k_2) calculated as the ratio of k_1 to the molar concentration of MNPs are shown in Table 2. As can be seen, all the nanocomposites in this reaction are catalytically active, but their activities vary greatly. Palladium nanocomposites have the highest activity (runs *3—5*, *10,* and *11*), while Au/$CoO_xH_y^{an}$ nanocomposites have the lowest activity (run *2*), in fact, the activities of these nanocomposites differ by tens of times. The other catalysts

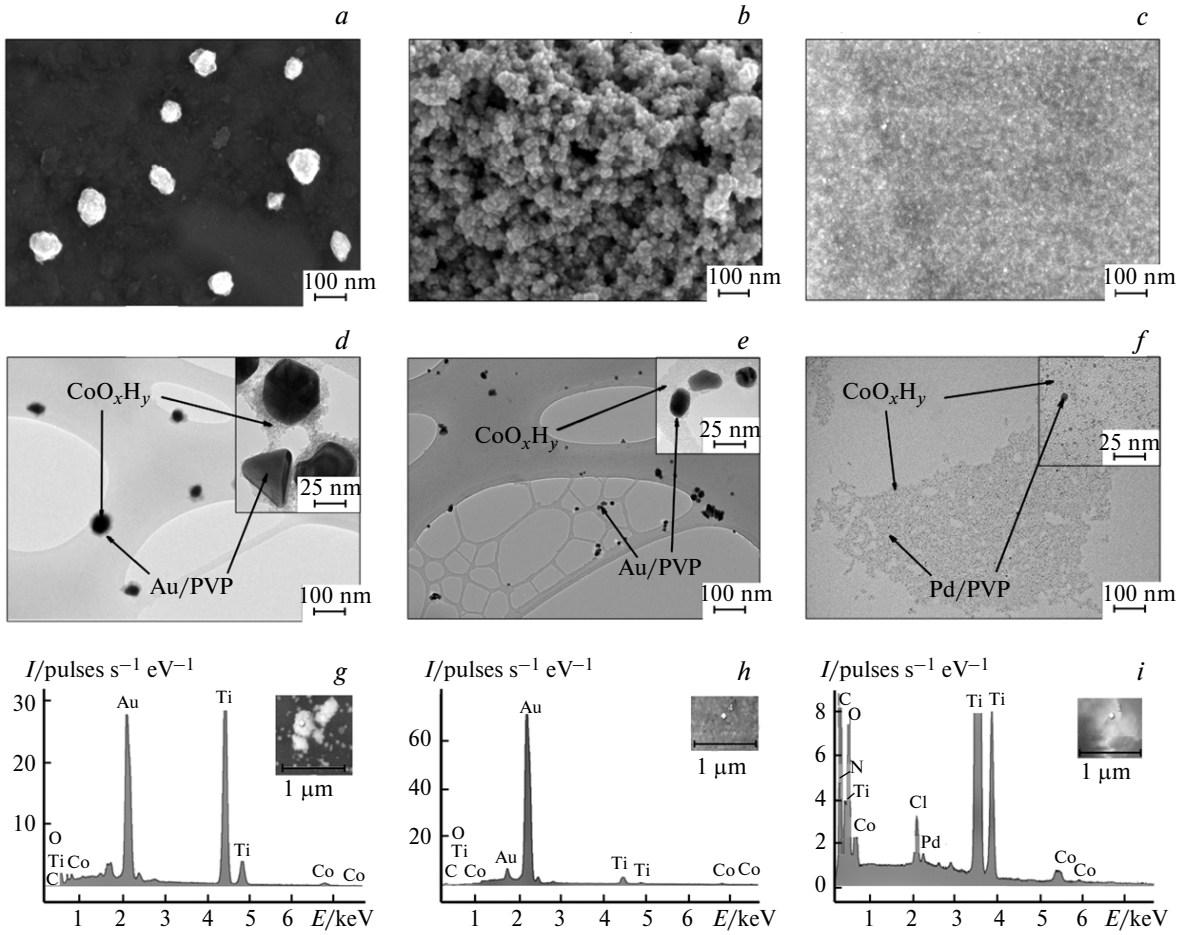

Fig. 11. SEM (*a*—*c*) and TEM images (*d*—*f*), as well as energy-dispersive spectra (*g*—*i*) of the Au@PVP/$CoO_xH_y^{an}$ and Pd@PVP/$CoO_xH_y^{an}$ nanocomposites obtained in runs *9* (*a*, *d*, *g*), *10* (*b*, *e*, *h*), and *12* (*c*, *f*, *i*) (see Table 1 and Experimental section). The insets in figures *g*—*i* show the areas of analysis. The Ti and Cu lines correspond to the support.

have intermediate activities. Matrices of nanocomposites, the CoO_xH_y (run *13*)[21] and CoO_xH_y/PVP particles (run *6*), which actually play a role of the support are considerably less active (see Table 1). It is clear that the catalytic activity of nanocomposites is caused by MNPs.

Scheme 2

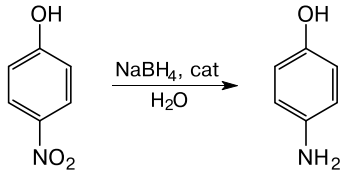

cat is catalyst

Nanocomposites obtained after the addition of metal ions to the $CoO_xH_y^{an}$ solutions (see Tables 1 and 2, runs *1*, *3*, *7*, *9*, *11*, and *14*) and the subsequent reduction (runs *2, 4*, *8*, *10*, *12*, and *15*) show different catalytic activity. Reduction leads to an increase in the reaction rate in the case of Pd-composites (runs *3*, *4*, *10, 11*) and Ag/CoO_xH_y (runs *14*, *15*) and to its decrease in the other cases. A particularly strong decrease in the activity (by a factor of seven) is observed for the composite Ag@PVP/CoO_xH_y. The reasons for the different effects of the second reduction step on the catalytic activity of nanocomposites are not entirely clear. One of the reasons may be the incomplete reduction of the metal ions by cobalt(II) oxide in runs *1*, *3*, *7*, *9*, *11*, and *14*, their *in situ* reduction with sodium borohydride under the reaction conditions to form the catalytically more active clusters and ultrafine MNPs. After the second reduction step, there are no the metal ions in the solution and, therefore, the reaction decelerated.

Stabilization of AuNPs with PVP, which prevents their agglomeration, leads to a sharp increase in the catalytic activity of nanocomposites (see Table 2, runs *2* and *10*). In the case of AgNPs and PdNPs, PVP also stabilizes individual small particles, but despite the fact that in the presence of PVP the catalyst has a larger specific surface, the reaction rate does not increase. Apparently, the PVP shell, which stabilizes MNPs, simultaneously reduces their

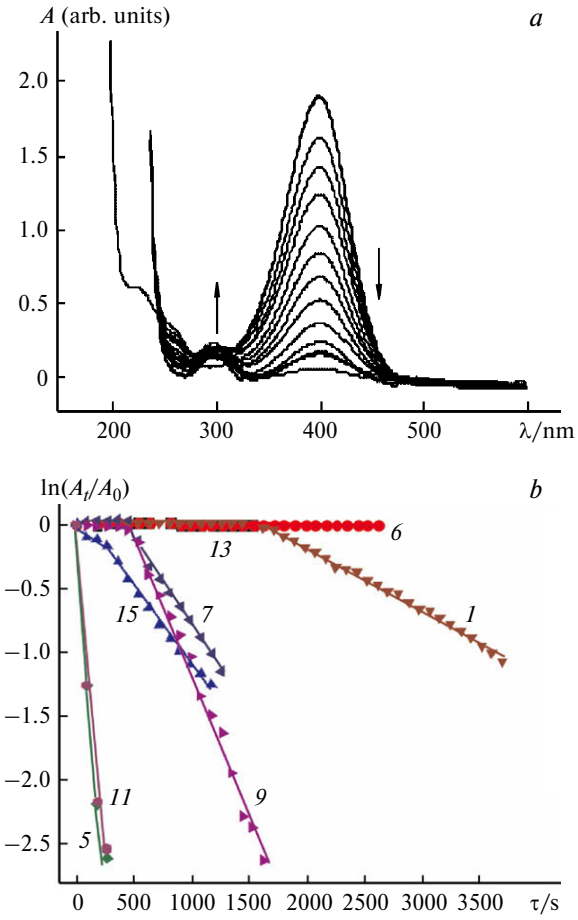

Fig. 12. The reduction of *p*-nitrophenol (0.1 mmol L^{-1}) with sodium borohydride (5 mmol L^{-1}), catalyzed by nanocomposites. *a*, Change in UV-Vis spectra of the reaction mixture after the addition of the the Au@PVP/$CoO_xH_y^{an}$ nanocomposite (see Tables 1 and 2, run *9*). *b*, Kinetic curves for nanocomposites obtained in runs *1* (Au (2 μmol L^{-1})/$CoO_xH_y^{an}$ (4 μmol L^{-1})), *5* (Pd^{an} (2 μmol L^{-1})/$CoO_xH_y^{an}$ (4 μmol L^{-1})), *6* (CoO_xH_y (4 μmol L^{-1})/PVP (26 μmol L^{-1})), *7* (Ag (2 μmol L^{-1})@PVP (26 μmol L^{-1})/CoO_xH_y (4 μmol L^{-1})), *9* (Au (2 μmol L^{-1})@PVP (26 μmol L^{-1})/$CoO_xH_y^{an}$ (4 μmol L^{-1})), *11* (Pd (2 μmol L^{-1})@PVP (26 μmol L^{-1})/$CoO_xH_y^{an}$ (4 μmol L^{-1})), *13** (CoO_xH_y (4 μmol L^{-1})), and *15** (Ag (2 μmol L^{-1})/$CoO_xH_y^{an}$ (4 μmol L^{-1})).

catalytic activity blocking the surface of MNPs to a certain extent and making it inaccessible to the reagents.

Table 2 also gives the catalytic activity of some palladium and silver nanocomposites obtained earlier in the reduction of *p*-nitrophenol under similar conditions. In general, the catalytic activity of the nanocomposites obtained in this work and of those synthesized earlier is comparable. This means that the CoO_xH_y matrix is neither a co-catalyst nor an inhibitor, but plays a role of an inert support of MNPs.

In conclusion, pseudo-homogeneous nanocatalysts, namely M/$CoO_xH_y^{(an)}$ (M = Au, Pd) and M@PVP/$CoO_xH_y^{(an)}$ (M = Ag, Au, Pd), were obtained by two-step electrosynthesis in DMF using atmospheric oxygen as a reagent and a mediator with potentials of its reduction to a superoxide radical anion. All the composites are formed according to the same scheme, which includes: (1) electrosynthesis of $CoO_xH_y^{(an)}$ particles followed by a redox reaction between CoO and Ag^+, Au^+, Pd^{2+} ions to give MNPs and CoO^+ and (2) oxygen-mediated reduction of CoO^+. In this case, CoO^+ ions play the role of a second mediator. Notably, the $CoO_xH_y^{(an)}$ matrix completely binds the nanoparticles M@PVP, partially or completely binds and stabilizes palladium and silver NPs, but neither binds nor stabilizes AuNPs. The obtained nanocomposites exhibit catalytic activity in the reduction of *p*-nitrophenol with sodium borohydride in water. The catalytic activity of Ag and Pd nanocomposites obtained in this work is comparable with the activity of other nanocomposites of these metals described earlier.

References

1. A. Eremenko, N. Smirnova, I. Gnatiuk, O. Linnik, N. Vityuk, Y. Mukha, A. Korduban, in *Nanocomposites and Polymers with Analytical Methods*, Ed. J. Cuppoletti, InTech, Rijeka, 2011, p. 51; DOI: 10.5772/18252.
2. S. M. Majhi, G. K. Naik, H.-J. Lee, H.-G. Song, C.-R. Lee, I.-H. Lee, Y.-T. Yu, *Sensors and Actuators*, *B*, 2018, **268**, 223.
3. J. Liu, S. Zou, S. Li, X. Liao, Y. Hong, L. Xiao, J. Fan, *J. Mater. Chem. A*, 2013, **1**, 4038.
4. R. P. Padbury, J. C. Halbur, P. J. Krommenhoek, J. B. Tracy, J. S. Jur, *Langmuir*, 2015, **31**, 1135.
5. D. Han, Z. Zhang, Z. Bao, H. Xing, Q. Ren, *Front. Chem. Sci. Eng.*, 2018, **12**, 24.
6. T. Hu, Y. Wang, Q. Liu, L. Zhang, H. Wang, T. Tang, W. Chen, M. Zhao, J. Jia, *Int. J. Hydrogen Energy*, 2017, **42**, 25951.
7. F.-Z. Song, Q.-L. Zhu, X. Yang, W.-W. Zhan, P. Pachfule, N. Tsumori, Q. Xu, *Adv. Energy Mater.*, 2018, **8**, 1701416.
8. A. B. Kuriganova, I. N. Leontyev, A. S. Alexandrin, O. A. Maslova, A. I. Rakhmatullin, N. V. Smirnova, *Mendeleev Commun.*, 2017, **27**, 67.
9. A. B. Kuriganova, D. V. Leontyeva, S. Ivanov, A. Bund, N. V. Smirnova, *J. Appl. Electrochem.*, 2016, **46**, 1245.
10. A. B. Kuriganova, N. V. Smirnova, *Mendeleev Commun.*, 2014, **24**, 351.
11. D. E. Doronkin, A. B. Kuriganova, I. N. Leontyev, S. Baier, H. Lichtenberg, N. V. Smirnova, J.-D. Grunwaldt, *Catal. Lett.*, 2016, **146**, 452.
12. P. S. Solmanov, N. M. Maximov, N. N. Tomina, A. A. Pimerzin, *Mendeleev Commun.*, 2018, **28**, 562.
13. A. V. Rassolov, G. N. Baeva, I. S. Mashkovsky, A. Yu. Stakheev, *Mendeleev Commun.*, 2018, **28**, 538.
14. S. W. Lee, J. T. Song, J. Kim, J. Oh, J. Y. Park, *Nanoscale*, 2018, **10**, 3911.
15. Z. Zhang, Q. Wu, X. Bu, Z. Hang, Z. Wang, Q. Wang, Y. Ma, *Bull. Korean Chem. Soc.*, 2018, **39**, 71.
16. M. Liu, W. Tang, Y. Xu, H. Yu, H. Yin, S. Zhao, S. Zhou, *Appl. Catal. A*, 2018, **549**, 273.

17. P. Supriya, B. T. V. Srinivas, K. Chowdeswari, N. V. S. Naidu, B. Sreedhar, *Mater. Chem. Phys.*, 2018, **204**, 27.
18. M. Gilanizadeh, B. Zeynizadeh, *Res. Chem. Intermed.*, 2018, **44**, 6053.
19. F. Aryanasab, *RSC Adv.*, 2016, **6**, 32018.
20. S. Jammi, S. Sakthivel, L. Rout, T. Mukherjee, S. Mandal, R. Mitra, P. Saha, T. Punniyamurthy, *J. Org. Chem.*, 2009, **74**, 1971.
21. V. V. Yanilkin, N. V. Nastapova, G. R. Nasretdinova, R. R. Fazleeva, Yu. N. Osin, *Electrochem. Commun*., 2016, **69**, 36.
22. V. V. Yanilkin, G. R. Nasretdinova, V. A. Kokorekin, *Russ. Chem. Rev*., 2018, **87**, 1080.
23. V. V. Yanilkin, N. V. Nastapova, R. R. Fazleeva, G. R. Nasretdinova, E. D. Sultanova, A. Yu. Ziganshina, A. T. Gubaidullin, A. I. Samigullina, V. G. Evtyugin, V. V. Vorob´ev, Yu. N. Osin, *Russ. J. Electrochem*., 2018, **54**, 265.
24. G. R. Nasretdinova, R. R. Fazleeva, Yu. N. Osin, V. G. Evtugin, A. T. Gubaidullin, A. Yu. Ziganshina, V. V. Yanilkin, *Electrochim. Acta*, 2018, **285**, 149.
25. V. V. Yanilkin, N. V. Nastapova, E. D. Sultanova, G. R. Nasretdinova, R. K. Mukhitova, A. Yu. Ziganshina, I. R. Nizameev, M. K. Kadirov, *Russ. Chem. Bull.*, 2016, **65**, 125.
26. V. V. Yanilkin, N. V. Nastapova, G. R. Nasretdinova, G. M. Fazleeva, L. N. Islamova, Yu. N. Osin, A. T. Gubaidullin, *ECS J. Solid State Sci. Technol.*, 2017, **6**, M143.
27. L. A. Dykman, V. A. Bogatyrev, S. Yu. Shchegolev, N. G. Khlebtsov, *Zolotye nanochastitsy. Sintez, svoystva, biomeditsinskoye primenenie* [*Gold Nanoparticles. Synthesis, Properties, Biomedical Application*], Nauka, Moscow, 2008, 319 pp. (in Russian).
28. V. V. Yanilkin, R. R. Fazleeva, G. R. Nasretdinova, N. V. Nastapova, Yu. N. Osin, *Butlerov Commun*., 2016, **46**, 128.
29. V. V. Yanilkin, R. R. Fazleeva, G. R. Nasretdinova, N. V. Nastapova, Yu. N. Osin, *New Mater., Compd. Appl*., 2018, **2**, 28.
30. V. V. Yanilkin, R. R. Fazleeva, G. R. Nasretdinova, N. V. Nastapova, Yu. N. Osin, *ECS J. Solid State Sci. Technol*., 2018, **7**, M55.
31. V. V. Yanilkin, R. R. Fazleeva, N. V. Nastapova, G. R. Nasretdinova, A. T. Gubaidullin, N. B. Berezin, Yu. N. Osin, *Russ. J. Electrochem*., 2018, **54**, 650.
32. I. P. Suzdalev, *Nanotekhnologiya: fiziko-khimiya nanoklasterov, nanostruktur i nanomaterialov* [*Nanotechnology: Physical Chemistry of Nanoclusters, Nanostructures, and Nanomaterials*], 2nd ed., Librokom, Moscow, 2009, 589 pp. (in Russian).
33. B. I. Kharisov, O. V. Kharissova, U. Ortiz-Méndez, *Handbook of Less-Common Nanostructures*, CRC Press, Taylor and Francis Group, Boca Raton, 2012, 836 pp.
34. A. M. Tafesh, J. Weiguny, *Chem. Rev*., 1996, **96**, 2035.
35. D. Astruc, *Nanoparticles and Catalysis*, Wiley-VCH, Weinheim, 2008, 663 pp.
36. P. Lara, K. Philippot, *Catal. Sci. Technol*., 2014, **4**, 2445.
37. V. V. Yanilkin, N. V. Nastapova, R. R. Fazleeva, G. R. Nasretdinova, E. D. Sultanova, A. Yu. Ziganshina, A. T. Gubaidullin, A. I. Samigullina, V. G. Evtugin, V. V. Vorobev, Yu. N. Osin, *Russ. Chem. Bull.*, 2018, **67**, 215.
38. P. Babji, V. L. Rao, *Int. J. Chem. Stud*., 2016, **4**, 123.
39. M. Yaseen, Z. Shah, R. C. Veses, S. L. P. Dias, É. C. Lima, G. S. dos Reis, J. C. P. Vaghetti, W. S. D. Alencar, K. Mehmood, *J. Anal. Bioanal. Technol*., 2017, **8**, 1.
40. N. Pradhan, A. Pal, T. Pal, *Colloids Surf., A*, 2002, **196**, 247.
41. P. Hervés, M. Pérez-Lorenzo, L. M. Liz-Marzán, J. Dzubiella, Y. Lu, M. Ballauff, *Chem. Soc. Rev*., 2012, **41**, 5577.

Received May 28, 2019;
in revised form September 18, 2019;
accepted November 18, 2019